The Development of a Statistical Forecast Model for Changma

SEUNG-EON LEE AND KYONG-HWAN SEO

Division of Earth Environmental System, Department of Atmospheric Sciences, Pusan National University, Busan, South Korea

(Manuscript received 1 January 2013, in final form 14 July 2013)

ABSTRACT

Forecasting year-to-year variations in East Asian summer monsoon (EASM) precipitation is one of the most challenging tasks in climate prediction because the predictors are not sufficiently well known and the forecast skill of the numerical models is poor. In this paper, a statistical forecast model for changma (the Korean portion of the EASM system) precipitation is proposed that was constructed with three physically based predictors. A forward-stepwise regression was used to select the predictors that included sea surface temperature (SST) anomalies over the North Pacific, the North Atlantic, and the tropical Pacific Ocean. Seasonal predictions with this model showed high forecasting capabilities that had a Gerrity skill score of ~0.82. The dynamical processes associated with the predictors were examined prior to their use in the prediction scheme. All predictors tended to induce an anticyclonic anomaly to the east or southeast of Japan, which was responsible for transporting a large amount of moisture to the southern Korean Peninsula. The predictor in the North Pacific formed an SST front to the east of Japan during the summertime, which maintained a lower-tropospheric baroclinicity. The North Atlantic SST anomaly induced downstream wave propagation in the upper troposphere, developing anticyclonic activity east of Japan. Forcing from the tropical Pacific SST anomaly triggered a cyclonic anomaly over the South China Sea, which was maintained by atmosphere–ocean interactions and induced an anticyclonic anomaly via northward Rossby wave propagation. Overall, the model used for forecasting changma precipitation performed well ($R = 0.85$) and correctly predicted information for 16 out of 19 yr of observational data.

1. Introduction

The long rainy season in the Korean Peninsula, called changma, accounts for 30% of the peninsula's annual precipitation. The large amount of rainfall during the changma period is accompanied by the changma front, which is a part of the quasi-stationary front of the East Asia summer monsoon (EASM). The corresponding quasi-stationary fronts over China and Japan are called mei-yu and baiu, respectively. Figure 1 shows climatological mean precipitation data from the Global Precipitation Climatology Project (GPCP) for the changma period (15 June–29 July). According to the GPCP, there are three strong precipitation cores (shaded) around the Asian continent: over the South Asia region (i.e., near the Arabian Sea and the Bay of Bengal), in the tropical western North Pacific (WNP), and in the EASM region. The planetary front of the EASM typically occurs over the Bay of Bengal and the South China Sea in May. The front migrates northward and forms a quasi-stationary front in June and July. In Fig. 1, a zonally elongated rainband can be seen in the EASM region (25°–40°N) and the rainfall maximum appears over the Korean Peninsula and southern Japan. The rainband moves gradually northward into North Korea in August. This general movement can be modified by a variety of external forcing factors (Lau et al. 2000), such as variation in sea surface temperatures (SSTs; Wang et al. 2000; Kim et al. 2009; Xie et al. 2009).

Mei-yu, changma, and baiu have similar characteristics because they are all subsystems of the EASM. However, some features of changma are different from mei-yu and baiu. Mei-yu is driven by the tropical monsoon air mass and the cold dry air mass from the continent of Asia, whereas baiu is formed by both the North Pacific subtropical high (NPSH) and the cold moist air mass over the Okhotsk Sea. The four air masses, which have different thermodynamic features, influence changma in complicated ways because changma forms in between mei-yu and baiu (Seo et al. 2011). Moreover, equatorial and polar air masses also affect changma intermittently (Seo et al. 2011).

Corresponding author address: Dr. Kyong-Hwan Seo, Dept. of Atmospheric Sciences, Pusan National University, Jangjeon-dong, Busan 609-735, South Korea.
E-mail: khseo@pusan.ac.kr

DOI: 10.1175/WAF-D-13-00003.1

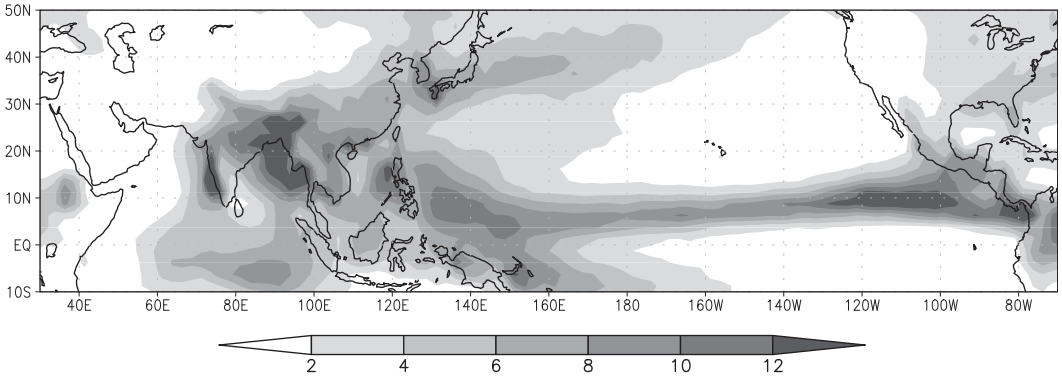

FIG. 1. Climatological mean precipitation data from the GPCP (mm day^{-1}) for the rainy changma season in the Korean Peninsula (15 June–29 July) during 1994–2011.

Ding and Chan (2005) summarized the EASM frontal features with two components: mei-yu (an area including southern China and the Yangtze River basin) and baiu (an area including changma). The western section of the front is characterized by a semitropical disturbance and a weak temperature gradient. It also has rather strong horizontal wind shear in the lower troposphere. On the other hand, the eastern section of the front has a baroclinic structure, strong vertical tilting toward an upper-level cold core, and a strong horizontal temperature gradient. These findings support the premise that mei-yu, changma, and baiu do not have the same structure and dynamics. Even though changma has different spatio-temporal characteristics compared to mei-yu and baiu, previous studies have focused primarily on mei-yu and baiu and their external forcings (e.g., Chang et al. 2000; Lau et al. 2000; Wang et al. 2000). Therefore, changma and its remote forcing processes need to be examined.

Interannual variations of the EASM are largely associated with remote forcing, rather than with processes in its own circulation system (Nitta 1987; Chang et al. 2000; Enomoto 2004; Ding and Wang 2005). Wang et al. (2000) showed that El Niño induced an anomalous anticyclone over the Philippine Sea, which influenced EASM circulation through a meridional tripole teleconnection pattern called the Pacific–Japan (PJ) teleconnection (Nitta 1987). In the extratropical region, a wave train zonally propagating from western Europe to North America through East Asia is called the circumglobal teleconnection (CGT; Ding and Wang 2005). The North Atlantic Oscillation (NAO) has been known to modify EASM rainfall through the CGT, especially during the winter to summertime period (Sung et al. 2006; Sun et al. 2008; Wu et al. 2009). Furthermore, a change in the subpolar jet caused by modified baroclinicity can modulate EASM precipitation through the atmospheric bridge (Lau et al. 2000; Lau and Weng 2002; Lau et al. 2004). For example, Lau et al. (2004) argued that the atmospheric bridge induced an SST front in the North Pacific along the Kuroshio during the summer, which was a one-way forcing from the atmosphere. However, recent studies have revealed that the atmosphere–ocean interaction along the SST front can be stronger than that of the atmospheric bridge (Qiu and Joyce 1992; Qiu and Kelly 1993; Qiu 2003). Within this context, Sampe et al. (2010) found a positive interaction between the ocean and atmosphere around the midlatitude SST front through a simplified model.

Even though EASM precipitation is important, current predictability is poor, even for the state-of-the-art model ensemble (Christensen et al. 2007). The multimodel ensemble (MME) has a higher predictability than does any single model prediction (Krishnamurti et al. 1999). However, poor Asian monsoon simulation by MME was noted in many previous studies (Sperber and Palmer 1996; Wang et al. 2004; Wang et al. 2009b). For example, Wang et al. (2009b) demonstrated that summer precipitation predictions by the MME in extratropical regions (20°–50°N, 100°–130°E) showed poor predictive capabilities (the correlation score ranged from 0.1 to 0.25) for a 23-yr (1981–2003) hindcast experiment.

Owing to the lack of prediction skill from the MME for Asian monsoons, an empirical model has been suggested for use in seasonal predictions. Shukla and Mooley (1987) constructed a statistical prediction model for precipitation over India. The predictability of tropical circulation and rainfall is higher than in the extratropical region since tropical ocean temperatures strongly determine the circulation and rainfall (Charney and Shukla 1981; Shukla 1998). However, some previous studies have tried to construct statistical seasonal prediction models for midlatitudes. These models include predictions of temperatures over North America (Livezey 1990), predictions of precipitation over China (Kim and Kim 2010), and predictions of circulation over the EASM region (Lee et al. 2008a,b). Importantly, Wu et al. (2009) suggested a physical–statistical regression model for an EASM

index using three predictors [an NAO index, an El Niño–Southern Oscillation (ENSO) developing index, and an ENSO decaying index] and showed higher prediction accuracy than the state-of-the-art MMEs. Their study also implied that an empirical model can be used as a real-time forecasting tool. Therefore, the construction of a statistical forecast model for changma precipitation may be valuable for enhancing prediction capabilities. Currently, there is no statistical forecast model for changma precipitation.

The aim of the current study was to construct a statistical forecast model for changma precipitation that was based on an understanding of the physical processes for selected predictors. We selected the potential predictors through statistical procedures and assessed the performance of the empirical model. Furthermore, we discuss the dynamical processes relevant to the selected predictors. This paper is organized as follows: section 2 describes the datasets and methodology, section 3 introduces the statistical forecast model and evaluates its performance, and section 4 discusses the dynamic processes in relation to the predictors. Finally, the summary and discussion are presented in section 5.

2. Data and methodology

a. Data

The observed daily precipitation dataset of the Korea Meteorological Administration (KMA) (1979–2012) was averaged for 60 stations, which were roughly uniformly distributed over all of South Korea. A few stations on two islands were included in the dataset. To define the changma index, station precipitation data were averaged from 15 June to 31 July (a time period that encompasses the typical changma period), and the typhoon days were removed beforehand so that the study would only consider large-scale dynamics. The days affected by typhoons were identified by checking typhoon tracks monitored by the KMA when typhoons were near the Korean Peninsula. To examine physical mechanisms in relation to select predictors for the prediction of changma precipitation, we used 300- and 850-hPa geopotential heights, 850- and 1000-hPa wind vectors, and mean sea level pressures (MSLPs) from the Global Reanalysis (R-2) daily dataset (1979–2012) of the National Centers for Environmental Prediction–Department of Energy (NCEP–DOE) (Kanamitsu et al. 2002). The dataset has a horizontal grid resolution of 2.5° × 2.5°. Additionally, the National Oceanic and Atmospheric Administration (NOAA) optimum interpolation (OI) SST version 2 high-resolution daily dataset (1982–2012) with a grid resolution of 0.25° × 0.25° from 1994 to 2012 (Reynolds et al. 2007) was also used. The OISST dataset was aggregated onto a 1° × 1° grid and averaged to a pentad dataset. Furthermore, the GPCP precipitation pentad dataset (1979–2012), which has a 2.5° × 2.5° grid from 1994 to 2012, was also used (Huffman et al. 1997). A recent study showed that precipitation strength in the EASM and the WNP summer monsoon changed abruptly around 1993/94, which led to a weakened subtropical jet and EASM circulation (Kwon et al. 2005). This implies that the basic state of the EASM changed near this period. Hence, we chose a hindcast period from 1994 to 2011 to avoid this interdecadal variation.

b. Methodology

We used a multiple linear regression method to build the model. Multiple linear regression has a single predictand similar to simple linear regression, but there is more than one predictor variable (Wilks 2006). The first step to building a prediction model is to set up the changma index as the predictand. Considering the importance of slowly varying the boundary forcing to changes in atmospheric circulation, global SSTs are the natural candidates to be predictor variables (Webster et al. 1998; Lau et al. 2000).

Most previous studies used monthly data for predictor variables. However, other time spans can be used; for example, from mid-April to mid-May. To find a more effective period for predictions, we used 5-day (pentad) averaged data and applied the moving-average technique. A moving average tends to reduce data errors and can help to build a stable prediction model. The moving-average window varied and spanned from 4 to 12 pentads so that each potential predictor had nine different time spans. The time coverage for each potential predictor ranged from 1994 to 2012, and the regression or composite analysis was conducted with data from 1994 to 2011 (18 yr). All variables were normalized so that the coefficients of the statistical model represented relative weightings. The following section describes the method used for selecting predictors.

1) SELECTING PREDICTORS

Figure 2 shows the spring SST anomalies (SSTAs) regressed against the changma index. Tropical central Pacific (CP) SSTAs showed strong negative anomalies for all of the specified periods, whereas weak positive SSTAs developed from March to May in the eastern Pacific. In early spring (Fig. 2a), weak positive anomalies were found near the WNP (10°–20°N, 120°E–180°) and negative values to the east of Japan (30°–40°N, 140°–160°E). However, the negative values became weak during late spring (Fig. 2c). Also, positive SSTAs appeared over the North Pacific (10°–40°N, 160°E–160°W)

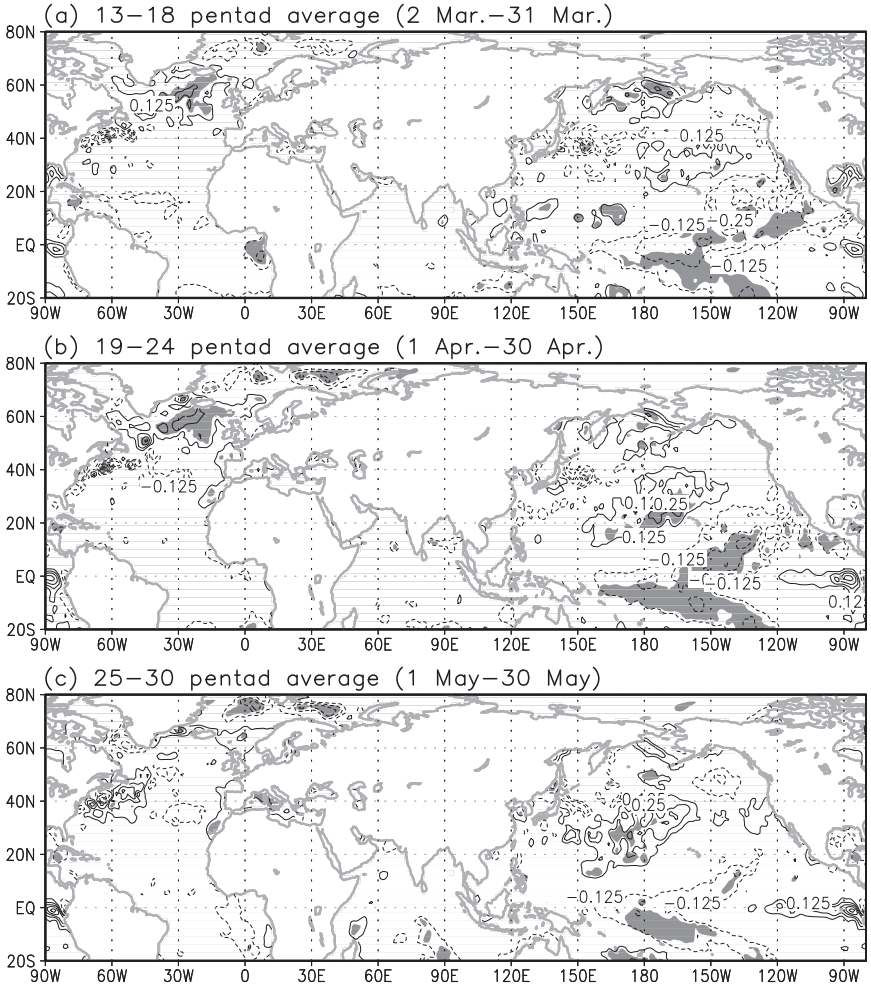

FIG. 2. SSTAs (K) regressed against the changma index (contour intervals of 0.125 K) for (a) 2 March–31 March, (b) 1–30 April, and (c) 1–30 May (all for 1994–2011). Shading indicates statistically significant regions at the 90% confidence level based on a Student's *t* test.

and their core gradually migrated northward. Another positive relationship with the changma index was observed in the North Atlantic Ocean, and this relationship was maintained until April. This statistically significant area over the North Atlantic Ocean was very similar to the significant correlation observed by Wu et al. (2009) with the NAO index. Over the Indian Ocean, there was only a weak signal, but this was selected as a potential predictor based on previous studies by Ding and Chan (2005) and Xie et al. (2009). By evaluating these relationships between SSTAs and the changma index, potential predictor candidates were determined (see the list of potential predictors in Table 1).

To screen potential predictor candidates, a forward-stepwise regression method was performed (Wilks 2006). Forward-stepwise regression starts with no predictors and tests are conducted with the addition of each predictor. Then, the predictor that satisfies certain criteria and improves the model the most is added to the model. This sequential process is repeated until the number of selected predictors is the same as the criterion. The number of predictors should be limited to three in order to prevent a large overfitting of coefficients (Wilks 2006). To test the prediction performance of selected predictors in the forward-stepwise regression, we applied the cross-validation method of Michaelsen (1987), whereby a leave-four-out strategy was used (Blockeel and Struyf 2002; Wu et al. 2009). For example, Blockeel and Struyf (2002) suggested the use of 70%–80% of the data to construct (or train) a regression model to prevent overfitting. The remaining data (20%–30%) can be used for model validation. Using the cross-validation method, a regression model was constructed with 14 yr of training data and the remaining consecutive 4 yr of data were

TABLE 1. List of potential predictor candidates considered in the forward-stepwise regression selection. All predictors except for the last one have nine different temporal segments according to a moving-average window varying from 4 to 12 pentads. The northern Pacific change was computed by the difference between 21–24- and 17–20-pentad averages. In the third column, the selected predictors are marked with an open circle and selected pentad numbers are shown.

Potential predictors	Areas	Selected predictor (pentad)
Niño-3	5°S–5°N, 150°–90°W	
Niño-3.4	5°S–5°N, 170°–120°W	
Niño-4	5°S–5°N, 160°E–150°W	
Central Pacific Niño	15°S–10°N, 160°–140°W	○ (19–22)
Western North Pacific 1	5°–25°N, 110°–140°E	
Western North Pacific 2	0°–15°N, 120°–160°E	
Tropical Western Pacific	10°S–15°N, 130°–160°E	
Northern Indian Ocean	0°–25°N, 50°–110°E	
North Atlantic 1	(55°–60°N, 40°–15°W)–(30°–45°N, 80°–40°W)	○ (20–23)
North Atlantic 2	(50°–65°N, 45°–10°W)–(30°–45°N, 80°–40°W)	
Korean Peninsula	20°–45°N, 120°–160°E	
Northern Pacific	20°–35°N, 160°–210°E	
Northern Pacific change	20°–35°N, 160°–210°E	○ (17–20) and (21–24)

used for model validation. This procedure (i.e., 4-yr validation in one step) was continued until all years in the hindcast period were validated.

2) CRITERIA

To prevent overfitting and to construct a robust statistical model, we applied three criteria in this study. The first criterion used in the forward-stepwise regression method was that predictors should have a high correlation to the changma index with a significance level better than 10%. The second criterion used was that the variance inflation factor (VIF), which measures multicollinearity between predictors, should be lower than 2. This diagnostic value was calculated as the reciprocal of the amount of variance in a predictor (or independent) variable that was not explained by the other predictor variables (Rogerson 2001; Lee et al. 2008a). The definition of VIF is explained further in the appendix. The third criterion used was that correlation coefficients between a potential predictor and other selected predictors should not be greater than 0.4. These three criteria were found to be effective in choosing predictors that had a high correlation with changma precipitation and were independent to each other.

3) FORECAST ASSESSMENT

To assess predictions, we used several verification methods including correlations, the root-mean-square error (RMSE), a contingency table, and a Gerrity score. A contingency table (also referred to as a cross tabulation or a cross tab) displays the relative frequency distribution of the predictors (Wilks 2006). Instead of displaying the frequency in the contingency table, we explicitly used the year for the corresponding forecast–observation pairing. Thus, this technique provided a useful way to check whether the forecasted value was correct. The Gerrity score [or a Gandin–Murphy skill score (GMSS)] was used to assess the overall forecasts, which is a tool that is recommended by the World Meteorological Organization (WMO 2010; Gerrity 1992). The definition of the GMSS is described in the appendix.

3. The seasonal prediction model

Through forward-stepwise regression, the following three SST predictors were selected: North Pacific change (NPC), North Atlantic 1 (NA1), and central Pacific Niño (CNINO) (see Table 1). One example of the model constructed is

$$\tilde{y} = 0.458(\mathrm{NPC}) + 0.413(\mathrm{NA1}) - 0.396(\mathrm{CNINO}) + 0.0136, \quad (1)$$

where $\tilde{y}$ represents the regressed values (Fig. 3, blue bars). The three predictors were computed in the spring without using summer information. Then, the model was used to predict summer (changma period) precipitation ($\tilde{y}$) using the coefficients. The coefficients of the specific regression model described above were computed using the hindcast period (1994–2009) and used for predictions during the years 2010–12. (For the validation of other years, the conventional 14 yr were used as training data and validation was performed on the remaining 4 yr.) From Fig. 3, we can see that precipitation for these 3 yr was well predicted. Again, the coefficients of the regression model varied for the different training periods, and forecasted precipitation for 1994–2012 in Fig. 3 was cross validated.

The prediction skill of the model for the years 1994–2012 was very high. The correlation coefficient between

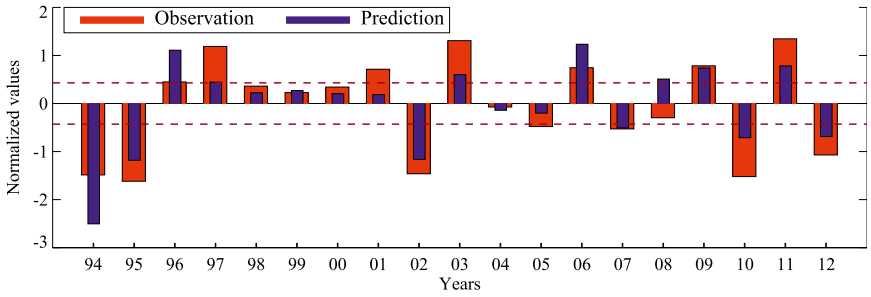

FIG. 3. Comparison of normalized precipitation predictions (blue bars) with observations (red bars). All years are cross validated (see the text for details). The dotted lines at +0.43 and −0.43 represent the threshold values for the tercile prediction. The correlation between predictions and observations was 0.85, the RMSE was 0.54, and the Gerrity score (GMSS) was 0.82.

the observed and predicted precipitation values was as high as ~0.85 and the RMSE was ~0.54. The top and bottom dotted lines shown in Fig. 3 denote the tercile prediction thresholds (i.e., the normalized values of ±0.43) representing below-normal, near-normal, and above-normal forecast areas. The 3 × 3 contingency table (Table 2) shows that there were 16 correct tercile prediction years, which amount to ~84.2% of the total years. The Gerrity score was computed to be ~0.82 (this score can have a maximum value of 1). To show how skillful is our model prediction, a climatological forecast is used as a reference and its skill score was estimated using the same cross-validation format. This analysis yielded a negative correlation (−0.29), a negative Gerrity score (−0.22), and a calculated RMSE of 1.61, which was almost 3 times larger than the RMSE for our forecast. These results suggest that the statistical model constructed in this study is capable of conducting skillful forecasts. The selected predictors had a high correlation with the changma index: 0.55 for NPC, 0.60 for NA1, and −0.57 for CNINO. The predictors had VIFs smaller than 1.21, and the correlations between the predictors were less than 0.251. Since the predictand and all predictors were normalized prior to constructing regression models, regression coefficients explicitly represent the degree to which the predictors contributed to the determination of predicted precipitation. The NPC had the highest coefficient, NA1 had the second highest coefficient, and CNINO had a negative coefficient, but the differences in magnitude were small.

In the model, the NPC predictor was represented as a time difference to capture the evolving property of the SST anomaly. In Fig. 2, the positive regressed SSTs in the North Pacific migrated northward. For example, the positive peak observed at 10°N during early spring (Fig. 2a) moved to 35°N in late spring (Fig. 2c). To consider this migrating behavior, the NPC was computed by a time difference between 21–24 and 17–20 pentad averages. Even though the SST predictors were computed during the spring for seasonal predictions, dynamics of the atmosphere and ocean can maintain the impact of SSTAs through the coming summer season. We demonstrate this in the next section.

4. The dynamic processes of predictors

To provide a robust and stable statistical prediction model, each selected predictor should have a dynamical process. For example, Webster et al. (1998) argued that the success of an empirical forecast would tend to support the theoretical basis of predictors. Changma forms at a higher latitude than mei-yu (in eastern China) and

TABLE 2. A contingency table for the validation of statistical precipitation prediction. The abscissa represents predictions and the ordinate represents observations. The above-normal, near-normal, and below-normal cases were determined by normalized values of ±0.43. The percentage at the bottom left is the ratio of the number of diagonally located years (i.e., correct tercile predictions) to the total number of years.

		Prediction		
		Above	Normal	Below
Observation	Above	1996, 1997, 2003, 2006, 2009, 2011	2001	
	Normal	2008	1998, 1999, 2000, 2004	
	Below		2005	1994, 1995, 2002, 2007, 2010, 2012
Percent = 84.2%				

baiu (in southern Japan), which indicates that changma may be more heavily influenced by midlatitude forcing. Recalling that tropical forcing has been known to enhance predictability (Shukla 1998), we evaluated whether or not midlatitude forcing can increase predictability through some dynamic processes.

a. Dynamic process of NPC

The NPC predictor is associated with change in North Pacific SSTs (referred to as NP; for 21–24 pentads, not the time difference). Figure 4a shows the regressed precipitation anomalies against 21–24-pentad-average NP variation during the changma period. A strong positive regressed anomaly (shading) was observed over the Korean Peninsula and the adjacent seas. Another positive area was seen over the South China Sea (SCS, 120°E) and the WNP (160°E) with cyclonic 850-hPa wind anomalies (vectors). Figures 4b and 4c show the regressed SSTAs against the NP for spring and the changma period, respectively. This SST variation was analyzed and thought to be the cause of the positive precipitation anomalies over the Korean Peninsula shown in Fig. 4a. In spring (Fig. 4b), most of the North Pacific in the Eastern Hemisphere was warm, except for the southern sea of the Korean Peninsula. Cold SSTAs were widely found in the tropical eastern Pacific. The warm region (10°–45°N in Fig. 4b) shrank during the summer, but it was maintained in the northern North Pacific (30°–45°N in Fig. 4c). The sustained warm region was located near the Kuroshio and it formed an SST front along 45°N, which tended to increase near-surface baroclinicity. The baroclinicity, in turn, strengthened the SST front through ''oceanic baroclinic adjustment'' (Nakamura and Shimpo 2004; Sampe et al. 2010).

To understand the oceanic baroclinic adjustment, the dynamics associated with storm tracks need to be considered. Nakamura and Shimpo (2004) and Nakamura et al. (2008) revealed the influence of the SST front on storm tracks using observation data and model simulations. Nakamura et al. (2004) also underlined the role of the SST front zone located under atmospheric baroclinicity and the subpolar jet (SPJ). The SPJ is an eddy-driven jet that is sustained by the conversion of available potential energy from mean flow into eddies (Vallis and Gerber 2008; Sampe et al. 2010). Eddy heat flux, which is comparable to eddy vorticity flux in the lower troposphere, intensifies the baroclinic growth of transient eddies and forms a deep storm track structure over the SPJ. Heat flux and vorticity flux have different roles in the storm track (Lau and Holopainen 1984; Lau and Nath 1991). The poleward heat flux accelerates eastward winds of the geostrophic flow in the lower troposphere and westward winds in the upper troposphere, which leads to a reduction in the vertical shear of the eastward flow along the storm track. On the other hand, the vorticity transport accelerates eastward winds throughout the troposphere over the storm track. Even though the two fluxes have different roles (the heat flux favors a baroclinic structure, whereas the vorticity flux favors a barotropic structure), the vorticity flux dominated in the upper troposphere. Thus, the combined effect of the two fluxes is to accelerate the eastward flow at all

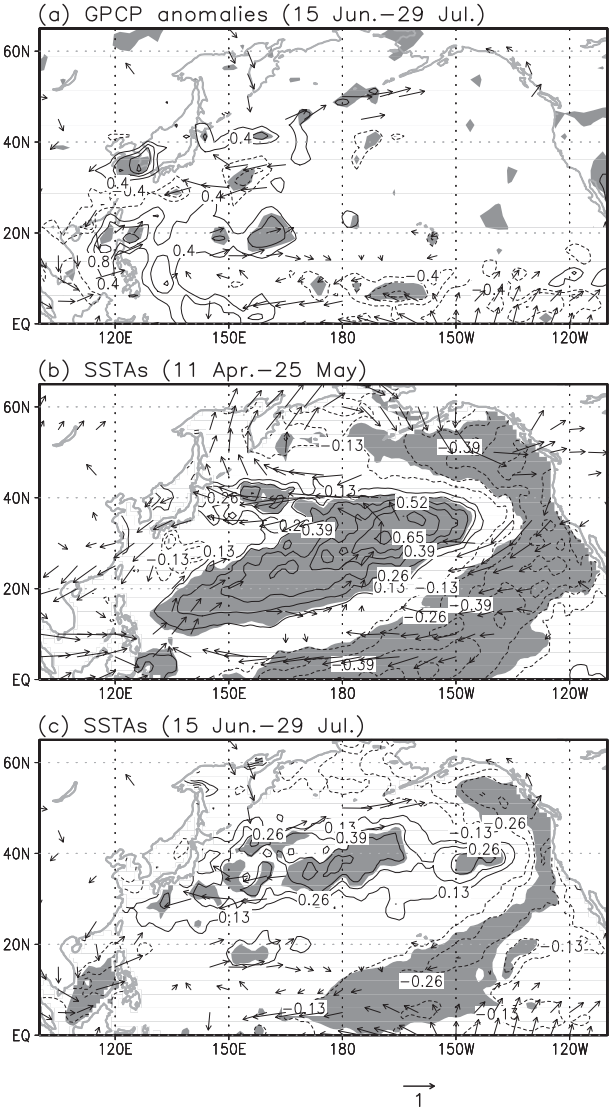

FIG. 4. The regressed (a) GPCP anomalies (contour intervals of 0.4 mm day^{-1}) from 15 June to 29 July, (b) SSTAs (contour intervals of 0.13 K) from 11 April to 25 May, and (c) SSTAs from 15 June to 29 July against the springtime NP time series (1994–2011). Shading indicates statistically significant regions at the 90% confidence level. The regressed 850-hPa winds (vectors, m s^{-1}) that were significant at the 90% confidence level are also plotted. The magnitude of the vectors is shown.

vertical levels in the midlatitudes. The intense eddy activity in the storm track transfers westerly momentum from the subtropics to the north and strengthens the SPJ. The eddy activity also induces the downward transport of westerly momentum and a low-level westerly jet by the dynamics explained above. In summary, the intense low-level baroclinic growth by poleward heat flux strengthens the SPJ and low-level westerly jet in the midlatitudes (Nakamura et al. 2004).

The oceanic baroclinic adjustment represents the mechanism by which the SST front zone effectively restores baroclinicity (Nakamura et al. 2008). Using simplified model simulations, Sampe et al. (2010) highlighted that cross-frontal differential sensible heat supply over the SST front was essential for maintaining the strong near-surface baroclinicity. The enhanced baroclinicity anchors a storm track, and the storm track maintains the near-surface westerlies through westerly momentum transport. The surface westerlies act to deepen the ocean mixed layer, which in turn contributes to the maintenance of the SST frontal zone. This positive feedback loop acts to transport heat from the ocean into higher latitudes by baroclinic eddies; that is, this positive feedback process operates in the earth's system to balance the heat budget.

Figure 5 shows the regressed MSLP anomalies against spring NP. In Fig. 5a, strong cyclonic anomalies were seen over the SCS and the WNP. These cyclonic anomalies were influenced by ENSO (Wang et al. 2000) according to the relationship between NP and tropical SSTAs as explained in section 3. However, in early summer (Fig. 5b), anticyclonic anomalies were located over the North Pacific (40°N), but these were not significant. An anticyclone could result from the continuous impact of the SST front. Figure 5c shows the anomalous westerlies along the northern border of the anomalous anticyclone in the North Pacific, which corresponded to the position of the SST front. These anomalous westerlies were also found in the regressed 200-hPa geopotential height anomalies (50°–55°N; data not shown). Through the role of the SST frontal zone as shown in Sampe et al. (2010), the low-level westerlies are strengthened by near-surface baroclinicity over the SST front zone. The westerlies also have a tropospheric deep structure. The persistent westerlies above the SST frontal zone likely strengthened the SPJ and induced an anticyclone anomaly over the northern Pacific (40°–50°N), which then led to the northward expansion of the NPSH. This was verified in the 850-hPa geopotential height anomaly composite (data not shown). Although the baroclinic eddies had a smaller time scale than changma, the oceanic front zone was maintained during spring and summer. Thus, the continuous forcing from the front zone modified the atmospheric circulation above the front

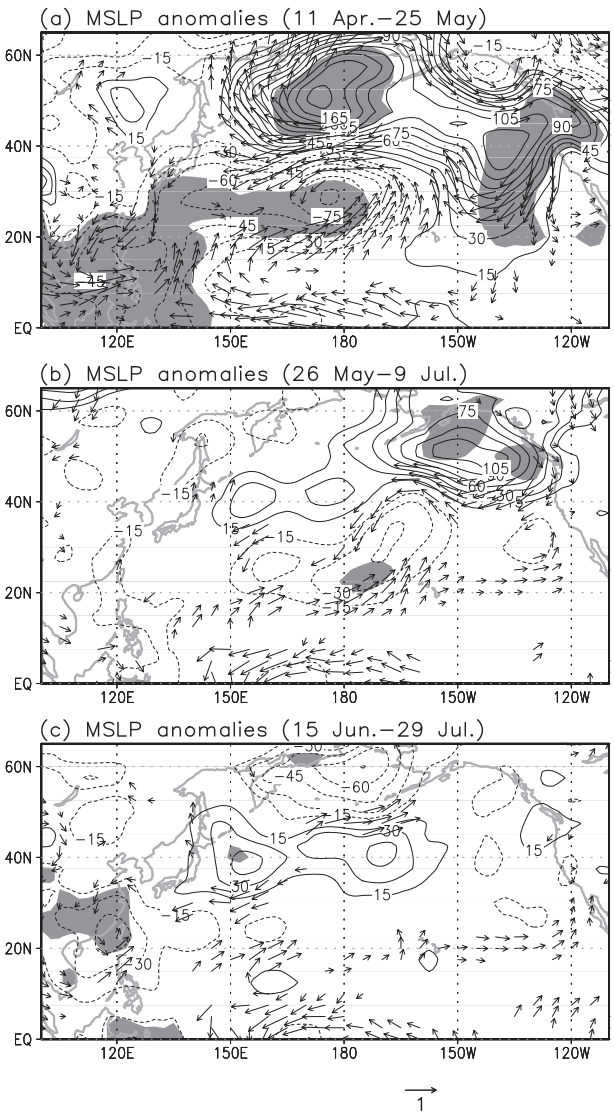

FIG. 5. The regressed MSLP anomalies (contour intervals of 15 hPa) against the springtime NP time series for (a) 11 April–25 May, (b) 26 May–9 July, and (c) 15 June–29 July (all for 1994–2011). Shading indicates statistically significant regions at the 90% confidence level. The regressed 1000-hPa winds (vectors, m s^{-1}) that were significant at the 90% confidence level are also plotted. The magnitude of the vectors is shown.

zone. The anomalous anticyclone circulation in Fig. 5c was responsible for transporting moist warm air into the southern Korean Peninsula in the lower troposphere and enhancing moist convection (Sampe and Xie 2010).

b. *Dynamic process of NA1*

Extratropical forcing over the Atlantic Ocean can affect changma precipitation (Fig. 6a). The NA1 represents tripolar cores over the Atlantic Ocean in spring (Fig. 6b), and these cores persist through the ensuing

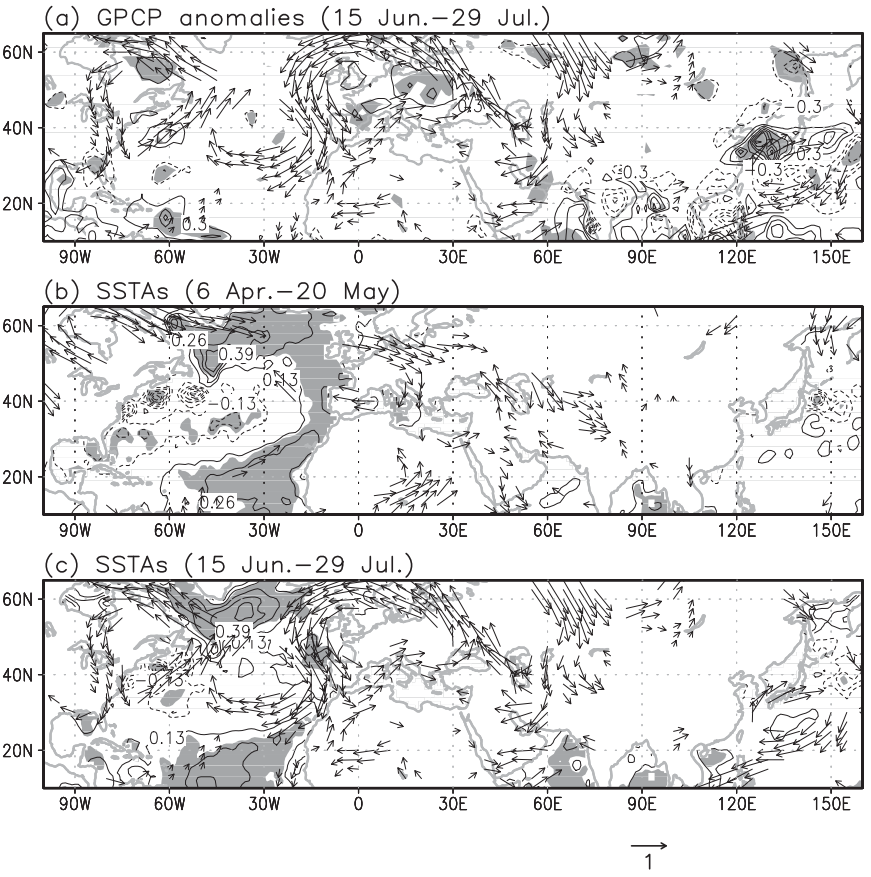

FIG. 6. The regressed (a) GPCP anomalies (contour intervals of 0.3 mm day^{-1}) from 15 June to 29 July, (b) SSTAs (contour intervals of 0.13 K) from 6 April to 20 May, and (c) SSTAs from 15 June to 29 July against the springtime NA1 time series (all for 1994–2011). Shading indicates statistically significant regions at the 90% confidence level. The regressed 850-hPa winds (vectors, m s^{-1}) that were significant at the 90% confidence level are also plotted. The magnitude of the vector is shown.

summer (Fig. 6c). This process is consistent with the previous study of Wu et al. (2009). Here, we used the two northern cores as a predictor, since these two cores showed a higher linear relationship than the tropical one. The boundary forcing from the SSTAs excited subpolar downstream Rossby wave energy dispersion across the Eurasian continent, leading to a strong EASM. This kind of wave-train-like teleconnection pattern has been found in previous studies (Ding and Wang 2005; Sung et al. 2006; Yamaura and Tomita 2011). Even though it is well known that the wintertime NAO exerts an influence on East Asia through a modification of the Asian jet waveguide (Branstator 2002; Yang et al. 2002), it has been recently discovered that the summertime NAO plays a role in forcing the wave train from the North Atlantic to East Asia (Wu et al. 2009; Yamaura and Tomita 2011). Sun et al. (2008) argued that the center of the NAO has shifted eastward since the late 1970s so that the NAO has greater impacts on East Asia through the Asian upper-level jet, which can induce anomalous summer air temperatures over East Asia. Summertime NAO forcing also modifies the EASM anomalous circulation, and triggers heavy rainfall over the Korean Peninsula and Japan within 2 days (Seo et al. 2012).

Figure 7 shows the composite difference (strong − weak cases) fields of 300- and 850-hPa geopotentials for the changma period. Strong cases are represented by the years with values larger than 0.75 in the summertime NA1 time series and weak cases are the ones that have values smaller than −0.75 in the time series. In Fig. 7a, anticyclonic anomalies appeared to the east and southeast of Japan, and this region had a barotropic structure (Fig. 7b). The barotropic Rossby wave train passing through the Eurasian continent down to Japan actually has two routes that emanate from the positive anomaly at 50°N, 0° over the North Atlantic. One of the routes

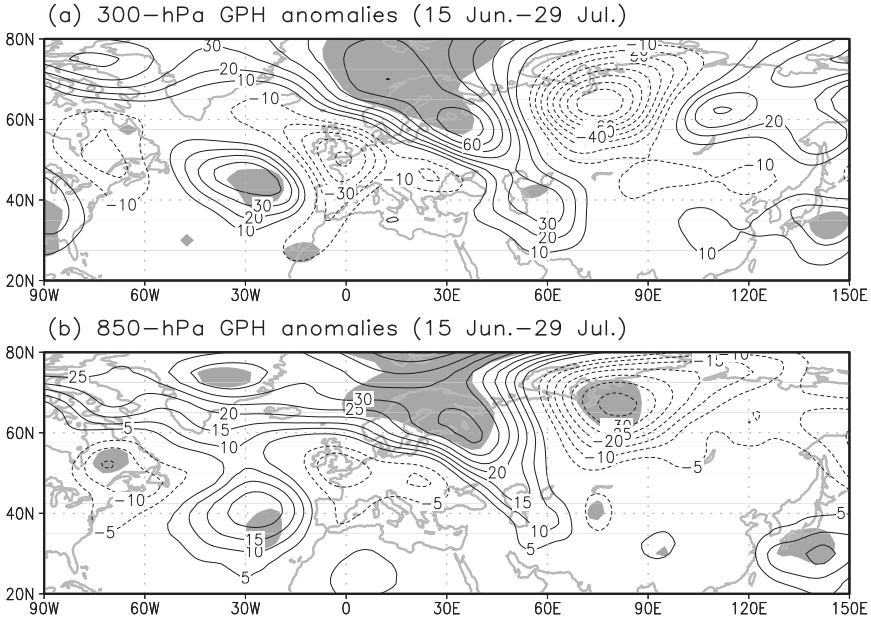

FIG. 7. Composite difference (strong − weak cases) fields for the (a) 300-hPa geopotential height anomaly (contour intervals of 10 m) and the (b) 850-hPa geopotential height anomaly (contour intervals of 5 m) against summertime (15 June–29 July) NA1 time series (during 1994–2011). Shading indicates statistically significant regions at the 90% confidence level. Composite criteria are ±0.75.

passes over the northern Eurasian continent around 60°N and the other route propagates in the midlatitude region around 30°–40°N. The former propagation corresponds to observations by Yamaura and Tomita (2011) and Wu et al. (2009) in which the upper-tropospheric Rossby waves that were amplified by the NAO propagated along the north Eurasian jet (60°N) to the east and changed their direction to south-southeastward around Lake Baikal because of the deceleration of the westerlies (Yamaura and Tomita 2011). The latter propagation was similar to the CGT (Ding and Wang 2005). The CGT has a zonal wavenumber-5 structure, except for during July when there is a relatively weak waveguide over the North Pacific and North American sector. Anomalous high pressure centers are situated over western Europe, European Russia, west-central Asia, East Asia, the North Pacific, and North America. In Fig. 7a, the three anomalous high pressure centers observed agreed relatively well with those of the CGT. Therefore, the NAO-forced SSTAs, which were maintained through the summer season, amplified upper-tropospheric Rossby waves that propagated toward the EASM region through the jet waveguides in the subpolar and midlatitude–subtropical regions. The wave propagation formed an anomalous anticyclonic circulation to the southeast of Japan, which helped to transport moist air toward the lower troposphere over the southern Korean Peninsula.

c. Dynamic process of the CNINO

The relationship between tropical SST and the EASM has been the subject of many studies in the last decade (Chang et al. 2000; Wang et al. 2000; Lee et al. 2008b). Figure 8 displays the regressed precipitation anomalies (CNINO for 19–22-pentad average) against the Korean precipitation index, where the sign of CNINO is reversed so as to express a positive contribution in the regression model, such as was shown in Eq. (1). Figures 9 and 10 show the regressed SSTAs and 850-hPa geopotential height anomalies, respectively, during the spring and summer with respect to the reversed 19–22-pentad-averaged CNINO index. These plots include three periods: spring (1 April–15 May), early summer (11 May–24 June), and changma (15 June–29 July). In spring, an extended anomalous cyclonic circulation from the SCS to the east of Japan generated negative rainfall anomalies and southward wind anomalies around the Korean Peninsula (Figs. 8a and 10a). However, during late spring and early summer the cyclonic anomalous circulation shrank (Fig. 10b), but it still existed over the SCS until the changma period (Fig. 10c). During the changma period, an anticyclonic anomalous circulation was evident to the east of Japan, which induced rainfall anomalies over the Korean Peninsula through southeasterly wind anomalies (Figs. 8c and 10c).

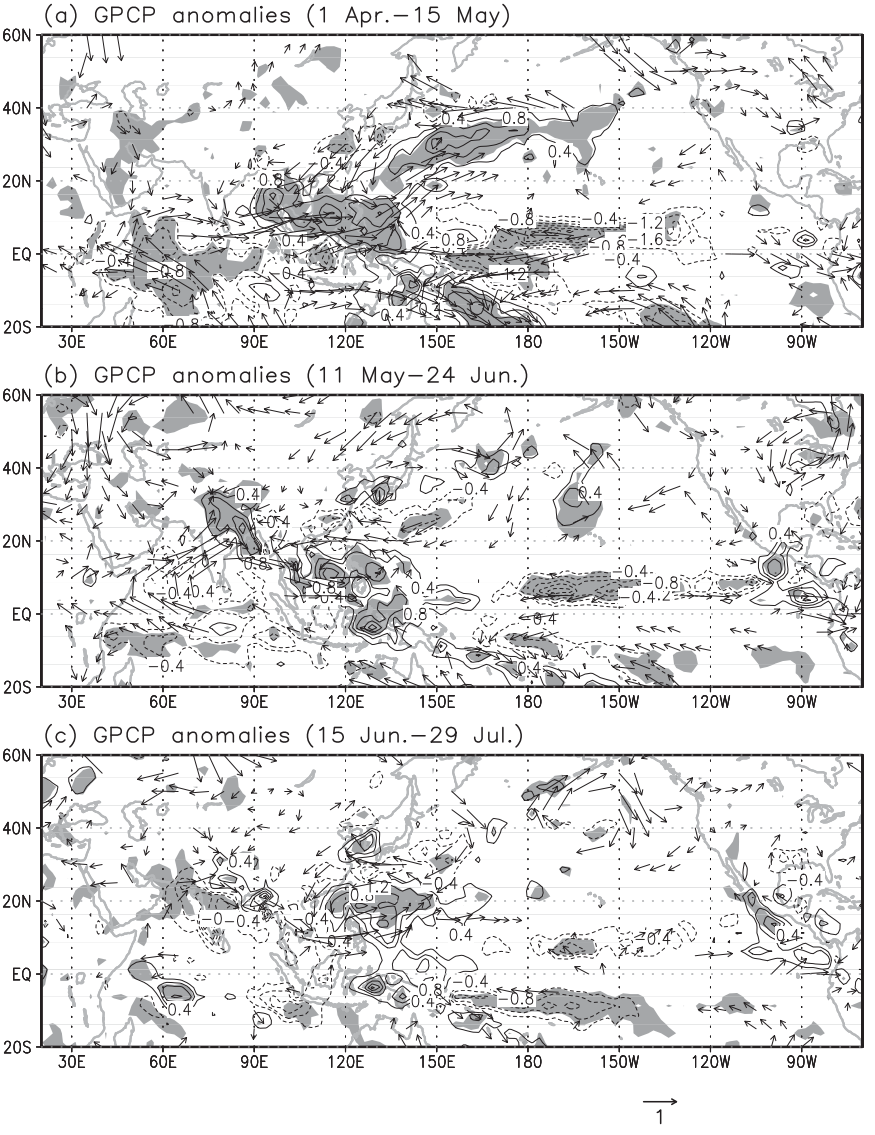

FIG. 8. The regressed GPCP anomalies (contour intervals of 0.4 mm day^{-1}) against the reversed springtime CNINO time series for (a) 1 April–15 May, (b) 11 May–24 June, and (c) 15 June–29 July (all for 1994–2011). Shading indicates statistically significant regions at the 90% confidence level. The regressed 850-hPa winds (vectors, m s^{-1}) that were significant at the 90% confidence level are also plotted. The magnitude of the vectors is shown.

The processes by which CNINO in the spring can affect changma rainfall are shown in Fig. 8c. The atmosphere–ocean interaction and local Hadley circulation could be keys to understanding the dynamic processes in relation to CNINO. During springtime, strongly negative SSTAs were found over the tropical Pacific and the Indian Ocean (Fig. 9a), whereas positive SSTAs were observed over the subtropical central Pacific. However, these patterns did not continue into the changma period. During the changma period, the negative SSTAs over the tropical Pacific weakened and extended slightly westward (Figs. 9b and 9c). Also, the negative SSTAs over the Indian Ocean showed a significant weakening during late spring and summer (Figs. 9b and 9c). In addition, the positive SSTAs over the North Pacific remained in the midlatitudes along 40°N (Fig. 9c), which was similar to Fig. 4c except that the center of the positive SSTAs was different (i.e., the peak was at 170°E in Fig. 4c and at 150°E and 160°W in Fig. 9c). Thus, the dynamics of NP and CNINO were different. Moreover, cold SSTAs developed in the SCS from early summer to the changma period (Figs. 9b and 9c).

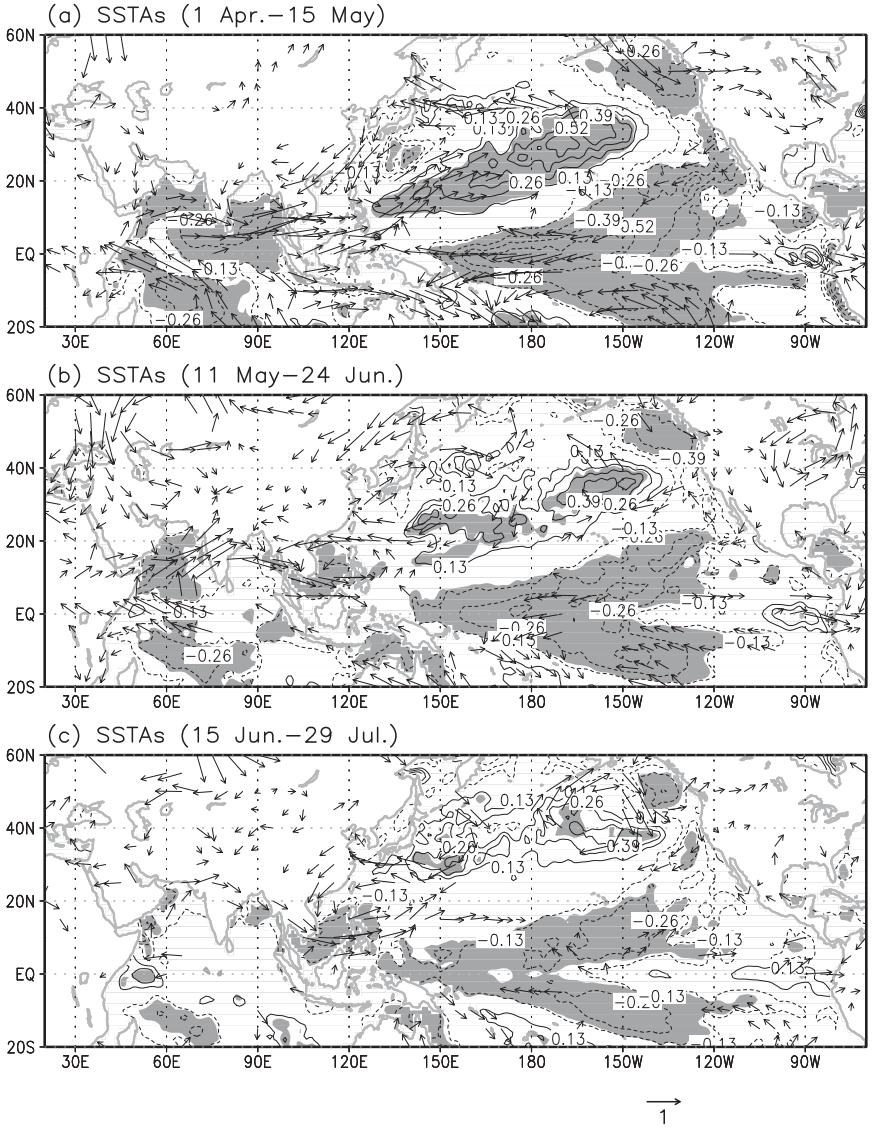

FIG. 9. The regressed SSTAs (contour intervals of 0.13 K) against the reversed springtime CNINO time series for (a) 1 April–15 May, (b) 11 May–24 June, and (c) 15 June–29 July (all for 1994–2011). Shading indicates statistically significant regions at the 90% confidence level. The regressed 850-hPa winds (vectors, $m\,s^{-1}$) that were significant at the 90% confidence level are also plotted. The magnitude of the vectors is shown.

In spring, strong easterlies in the tropical lower troposphere (Fig. 10a) enhanced rainfall on the western Walker circulation limb and formed positive rainfall anomalies in the eastern Philippine Sea (Fig. 8a). The enhanced rainfall anomalies in the western Pacific that were associated with midtropospheric heating resulted in cyclonic Rossby anomalies over the western Pacific (hereafter WNPC is used for the cyclonic Rossby anomalies) that were reminiscent of the Matsuno–Gill circulation response (Gill 1980; Wang et al. 2000). Wang et al. (2000) claims that the southwest–northeast-oriented anomalous anticyclone activity induces warm SSTs in the East Asian marginal seas and cold SSTs over the western Pacific by modifying the trade winds. These two SSTA fields (the warm SSTA over the East Asian seas and the cold SSTA in the western North Pacific) are as important as the central tropical Pacific SSTAs because of an atmosphere–ocean positive feedback. The positive feedback mechanism between the WNPC and the underlying dipolar SSTAs maintains the strength of the WNPC through early summer (Wang et al. 2000). Furthermore, the variation of the WNPC could be influenced

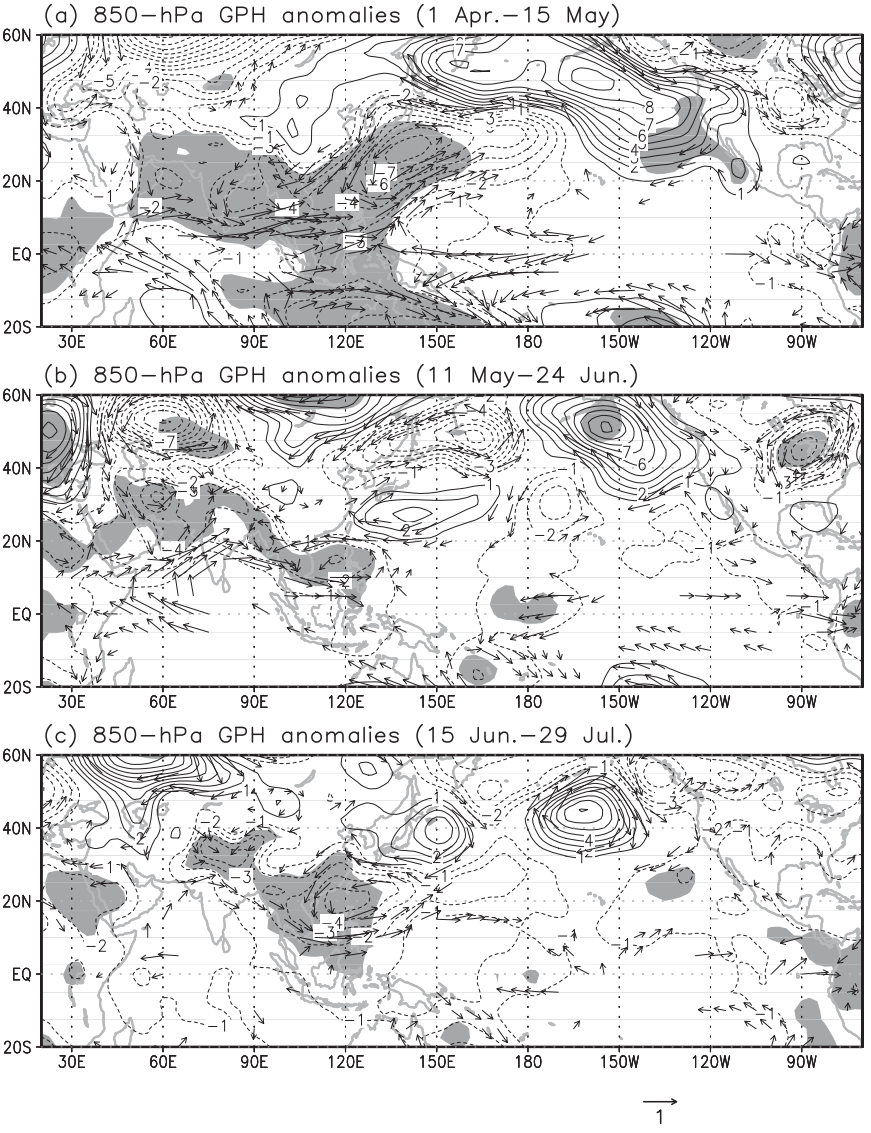

FIG. 10. The regressed 850-hPa geopotential height anomalies (contour intervals of 1 m) against the reversed springtime CNINO time series for (a) 1 April–15 May, (b) 11 May–24 June, and (c) 15 June–29 July (all for 1994–2011). Shading indicates statistically significant regions at the 90% confidence level. The regressed 850-hPa winds (vectors, m s^{-1}) that were significant at a 90% confidence level are also plotted. The magnitude of the vectors is shown.

by local Hadley circulation. The tropical easterlies shown in Fig. 8b can induce off-equatorial surface ocean transport by Ekman transport, resulting in cold SSTAs along the equator. The cold SSTAs can weaken the above-mentioned Hadley circulation and then induce weaker westward expansion of the NPSH to the WNP area than is normal (Chang et al. 2000). The WNPC also helps the concurrent development of cold SSTAs in the SCS by Ekman-induced upwelling (Fig. 8c) (Chang et al. 2000). In summary, two processes including atmosphere–ocean interactions and local Hadley circulation can form favorable conditions for sustaining the WNPC through summer. The sustained WNPC forms the anticyclonic anomaly to the east of Japan (Fig. 10) through a PJ-like teleconnection. Therefore, the spring CNINO acts to maintain the WNPC, which transfers wave energy northeastward and forms an anticyclonic circulation to the east of Japan. The WNPC and the associated anticyclonic circulation transport moist air toward the southern Korean Peninsula and produce positive rainfall anomalies there.

5. Summary and discussion

Developing a statistical forecast model for changma precipitation is of central importance because precipitation forecasts for the Korean Peninsula derived from contemporary global climate models (GCMs) perform poorly. Most previous attempts to construct statistical regression models in the region were for the South Asian summer monsoon or the EASM, which are not identical to changma precipitation. Given that previous works suggest that regression models can have higher prediction capabilities than the MME, the need to build a statistical forecast model for South Korea has increased. The prediction capability of an empirical model can be guaranteed to some extent by choosing potential predictors that are linked to dynamical processes. In this sense, potential predictor candidates are computed using slowly varying boundary conditions (i.e., SSTAs) over tropical and extratropical regions ahead of the changma season.

This paper developed a statistical seasonal forecast multiple regression model for changma precipitation that was constructed with SSTAs over the North Pacific (NPC), North Atlantic (NA1), and central tropical Pacific (CNINO). These predictors were selected by a forward-stepwise regression method using three criteria that minimized overfitting. The prediction model showed high performance capabilities ($R = 0.85$ and GMSS = 0.82). Only 3 out of 19 yr of observational data were incorrectly predicted by the model. Since days affected by typhoons were removed beforehand, the prediction model only considers large-scale dynamics, a feature that has not been examined in previous studies.

The three predictors selected for use in the model were related to the following dynamical processes:

1) The regression analysis for springtime NP SSTAs demonstrated the importance of a zonal SST front zone in the North Pacific because of the presence of positive atmosphere–ocean feedback. The positive feedback enhanced near-surface baroclinicity and trapped storm tracks. The storm tracks in turn strengthened the SST front. These processes sustained and induced the northwestward expansion of the NPSH.
2) As previous studies have identified, NAO forcing can modify EASM circulation through barotropic Rossby wave propagation. The Rossby waves generated over the North Atlantic propagated toward the EASM in two paths through a jet stream waveguide. The waves propagating along the southern route (~30°N) induced three anticyclonic anomalies whose positions were similar to those of CGT. The easternmost anticyclonic anomaly was located to the southeast of Japan, which induced moist southerly flows to the Korean Peninsula.
3) The reversed CNINO was characterized by strong cold SSTAs over the central tropical Pacific, which were accompanied by tropical easterlies directed toward the Maritime Continent. The winds enhanced rainfall over the eastern Philippine Sea and triggered a Matsuno–Gill-type response. The diabatic heating induced a PJ-like teleconnection pattern with cyclonic anomalies over the WNP and anticyclonic anomalies to the east of Japan. The latter formed favorable conditions for the northward influx of moist air to the Korean Peninsula.

The above three main processes are illustrated in Fig. 11. The three SST predictors affecting changma precipitation were located over the global area (i.e., in both the tropics and the extratropics), which implies the existence of remote effects on changma precipitation variability. The formation of the anticyclonic circulation anomaly to the east or southeast of Japan was found to be the most important factor for interannual changma variation. A recent study by Seo et al. (2012) also demonstrated that the northward or northwestward intensification/expansion of the NPSH caused an extraordinary increase in changma precipitation during the summer of 2011. Interestingly, the EASM response to global warming from the fifth phase of the Coupled Model Intercomparison Project (CMIP5) data exhibits a similar northwestward intensification of the NPSH in future climate scenarios (Seo et al. 2013). In their study, precipitation is anticipated to increase moderately over the northern part of the Korean Peninsula by the end of twenty-first century. The remote forcing from the tropical Pacific Ocean and the North Atlantic Ocean has been examined previously within the context of the EASM. However, this is the first study that we are aware of that highlights that positive atmosphere–ocean feedback over the North Pacific SST front can increase changma precipitation. The anomalous anticyclone to the east or southeast of Japan in the present study needs to be differentiated from the so-called WNPSH (western North Pacific subtropical high) (Wang et al. 2013), which is a westward intensification of the NPSH that mostly affects the mei-yu part of the EASM.

In this study, springtime SST patterns regressed onto the NP and CNINO indices (Figs. 4b and 9a, respectively) appeared to be similar and the springtime correlation between the two indices was strongly negative ($R = -0.76$; CNINO index not reversed). In El Niño (La Niña) years, the tropical eastern and central Pacific is obviously warm (cold), whereas cold (warm) SSTAs are located from the WNP to the extratropical central Pacific (Lau et al. 2000; Wang et al. 2009a). Because of this pattern, the NP region has cold SSTAs that show

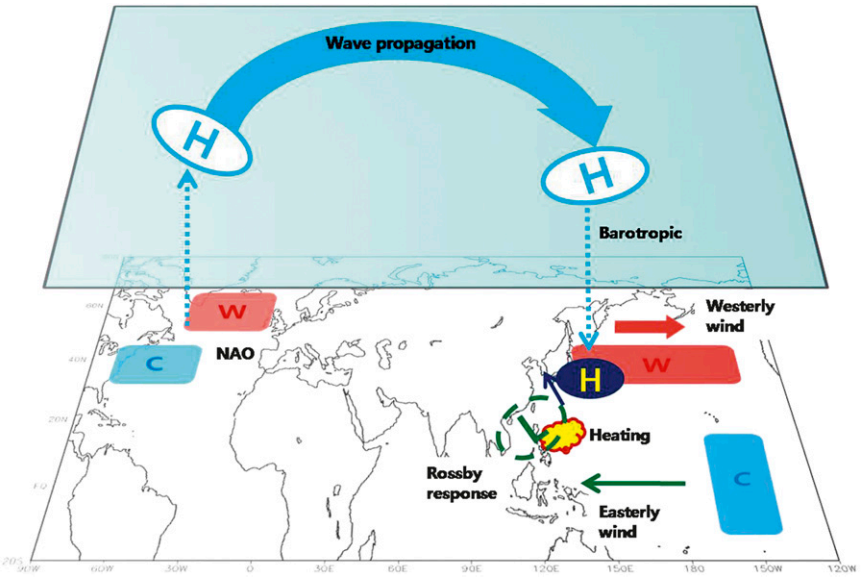

FIG. 11. A schematic diagram illustrating the dynamic processes associated with the three predictors (i.e., SST anomalies over the central North Pacific, the North Atlantic, and the tropical central/eastern Pacific). In the bottom panel, the red (blue) shading denotes the positive (negative) SST anomalies. The anticyclonic circulation anomaly to the east or southeast of Japan (which is the most crucial component for modulating interannual changma precipitation variability) is plotted with dark blue shading.

a negative relationship with the tropical El Niño SST anomalies. However, these two anomalies exhibit different dynamical properties during the summer. Calculation of lead–lag correlations for the CNINO and NP indices (e.g., with lags from −12 to 0 months) against the fixed summer changma index (data not shown) show that the correlation between the CNINO and changma indices has a biennial variation, similar to the findings of Yun et al. (2009) and Wang et al. (2001). This biennial characteristic implies that CNINO presents the typical tropical ENSO. On the other hand, no biennial variation was observed in the correlation between the NP and changma indices. Moreover, the correlation between CNINO and NP became weak in the summer. Lau et al. (2000, 2004) argue that the leading two empirical orthogonal function modes of the NP SST have a weak relationship with ENSO in the summer. Hence, the above analyses imply that NP evolves differently from CNINO. Again, the NP is influenced by equatorial Pacific SSTAs in spring, but its own dynamics become strong in summer, which makes it reasonable to select NPC and CNINO as different predictors.

A decadal change in precipitation patterns during 1993/94 makes it difficult to determine stable predictors and to obtain higher forecasting skill (Kwon et al. 2005). In this paper, the latest 19 yr (1994–2012) of data were used. While this period was somewhat short for constructing a stable and reliable statistical forecast model, this limitation was overcome by the value of identifying all predictors that were greatly involved in the specific dynamic processes. Through this investigation, the most important factors that determine interannual variation in changma precipitation can be understood. Additionally, this level of understanding may be useful for constructing longer-duration models in the future.

There are several other factors that may impact changma precipitation, such as snow cover, the Arctic oscillation, the Madden–Julian oscillation, and Tibetan Plateau warming (Webster et al. 1998; Gong and Ho 2003; Ding and Chan 2005; Wang et al. 2008; Kim et al. 2009; Yim et al. 2010). These boundary forcings or atmospheric phenomena will be examined in more detail in future studies to enhance the predictability of statistical forecast models. Moreover, an ensemble built with constructed models may further increase our prediction capabilities.

Acknowledgments. This work was funded by the Korea Meteorological Administration (KMA) Research and Development Program under Grant CATER 2012–3071. We are grateful to three anonymous reviewers for their helpful comments and suggestions that improved the paper. The authors would also like to acknowledge support from the Korea Institute of Science and Technology Information (KISTI).

APPENDIX

Computation of the VIF and Gerrity Score (GMSS)

The variance inflation factor (VIF) quantifies how a predictor variable is related to other predictor variables in a multiple regression equation (Rogerson 2001; Lee et al. 2008a), and it is calculated as the reciprocal of the amount of variance in a predictor variable that is not explained by the other predictor variables:

$$\mathrm{VIF} = \frac{1}{1 - R^2}, \tag{A1}$$

where R^2 is the coefficient of determination obtained by regressing the selected predictor variable onto the remaining predictor variables. Because the coefficient of determination is the ratio of the explained variance to the total variance, a small VIF indicates that the remaining predictor variables explain a small proportion of the selected predictor variable. Thus, VIF provides information on the linearity between the selected predictor variable and the other predictor variables (i.e., multicollinearity). Because multicollinearity should be avoided when constructing an empirical model to avoid overfitting, a low VIF is required when selecting predictor variables.

The Gerrity score [or Gandin–Murphy skill score (GMSS)] is computed from a scoring matrix that rewards correct forecasts and penalizes incorrect ones (Livezey 2003; Wilks 2006; WMO 2010):

$$\mathrm{GMSS} = \sum_{i=1}^{I}\sum_{j=1}^{J} p(y_i, o_j) s_{i,j}, \tag{A2}$$

$$p(y_i, o_j) = p(y_i \mid o_j) p(o_j)$$

$$= \frac{n_{i,j}}{\sum_{i=1}^{I} n_{i,j}} \frac{n_{i,j}}{\sum_{i=1}^{I}\sum_{j=1}^{J} n_{i,j}}, \quad (i = 1, \ldots, I;\ j = 1, \ldots, J), \tag{A3}$$

$$D(j) = \frac{1 - \sum_{r=1}^{j} p(o_r)}{\sum_{r=1}^{j} p(o_r)}, \quad (j = 1, \ldots, J-1), \tag{A4}$$

$$s_{i,j} = \frac{1}{J-1}\left[\sum_{r=1}^{i-1}\frac{1}{D(r)} + \sum_{r=j}^{J-1} D(r) - (j-i)\right], (1 \le i < j \le J), \quad \text{and} \tag{A5}$$

$$s_{j,j} = \frac{1}{J-1}\left[\sum_{r=1}^{j-1}\frac{1}{D(r)} + \sum_{r=j}^{J-1} D(r)\right], \quad (j = 1, \ldots, J), \tag{A6}$$

where GMSS is the Gerrity skill score, $p(y_i, o_j)$ is the joint distribution, and $s_{i,j}$ and $s_{j,j}$ are the scoring matrix. The subscript i in y_i is the forecast category and j in o_j is the observation category. Parameter $n_{i,j}$ is the number of the ith column and the jth row in the contingency table. In addition, $D(j)$ is the ratio of probability and r is a dummy variable for summation. The joint distribution [Eq. (A3)] is a conditional probability that represents the probability of a forecast occurrence when an observation occurs. The scoring matrix [Eqs. (A4), (A5), and (A6)] places greater weighting on the diagonal ones [called hits; Eq. (A6)] and low or negative coefficients to nondiagonal ones [called false alarms, misses, and correct rejections, respectively, depending on the matrix position from Eq. (A5)], because Eq. (A5) has the term "$-(j - i)$" (Wilks 2006). The maximum GMSS value is 1.

REFERENCES

Blockeel, H., and J. Struyf, 2002: Efficient algorithms for decision tree cross-validation. *J. Mach. Learn. Res.,* **3,** 621–650, doi:10.1162/jmlr.2003.3.4-5.21.

Branstator, G., 2002: Circumglobal teleconnections, the jet stream waveguide, and the North Atlantic Oscillation. *J. Climate,* **15,** 1893–1910.

Chang, C. P., Y. Zhang, and T. Li, 2000: Interannual and interdecadal variations of the East Asian summer monsoon and tropical Pacific SSTs. Part I: Roles of the subtropical ridge. *J. Climate,* **13,** 4310–4325.

Charney, J. G., and J. Shukla, 1981: Predictability of monsoons. *Monsoon Dynamics,* J. Lighthill, Ed., Cambridge University Press, 99–110.

Christensen, J. H., and Coauthors, 2007: Regional climate projections. *Climate Change 2007: The Physical Science Basis,* S. Solomon et al., Eds., Cambridge University Press, 847–940.

Ding, Q., and B. Wang, 2005: Circumglobal teleconnection in the Northern Hemisphere summer. *J. Climate,* **18,** 3483–3505.

Ding, Y., and J. C. L. Chan, 2005: The East Asian summer monsoon: An overview. *Meteor. Atmos. Phys.,* **89,** 117–142.

Enomoto, T., 2004: Interannual variability of the Bonin high associated with the propagation of Rossby waves along the Asian jet. *J. Meteor. Soc. Japan,* **82,** 1019–1034.

Gerrity, J. P., Jr., 1992: A note on Gandin and Murphy's equitable skill score. *Mon. Wea. Rev.,* **120,** 2707–2712.

Gill, A. E., 1980: Some simple solutions for heat induced tropical circulation. *Quart. J. Roy. Meteor. Soc.,* **106,** 447–462.

Gong, D.-Y., and D.-H. Ho, 2003: Arctic oscillation signals in the East Asian summer monsoon. *J. Geophys. Res.,* **108,** 4066, doi:10.1029/2002JD002193.

Huffman, G. J., and Coauthors, 1997: The Global Precipitation Climatology Project (GPCP) combined precipitation dataset. *Bull. Amer. Meteor. Soc.,* **78,** 5–20.

Kanamitsu, M., W. Ebisuzake, J. Woolen, S.-K. Yang, J. J. Hnilo, M. Fiorino, and G. L. Potter, 2002: NCEP–DOE AMIP-II Reanalysis (R-2). *Bull. Amer. Meteor. Soc.,* **83,** 1631–1643.

Kim, J.-E., S.-W. Yeh, and S.-Y. Hong, 2009: Two types of strong northeast Asian summer monsoon. *J. Climate,* **22,** 4406–4417.

Kim, M.-K., and Y.-H. Kim, 2010: Seasonal prediction of monthly precipitation in China using large-scale climate indices. *Adv. Atmos. Sci.,* **27,** 47–59, doi:10.1007/s00376-009-8014-x.

Krishnamurti, T. N., C. M. Kishtawal, T. E. La Row, D. R. Bachiochi, Z. Zhang, C. E. Williford, S. Gadgil, and S. Surendran, 1999: Improved weather and seasonal climate forecasts from multimodel superensemble. *Science,* **285,** 1548–1550, doi:10.1126/science.285.5433.1548.

Kwon, M.-H., J.-G. Jhun, B. Wang, S.-I. An, and J.-S. Kug, 2005: Decadal change in relationship between East Asian and WNP summer monsoons. *Geophys. Res. Lett.,* **32,** L16709, doi:10.1029/2005GL023026.

Lau, K.-M., and H. Weng, 2002: Recurrent teleconnection patterns linking summertime precipitation variability over East Asia and North America. *J. Meteor. Soc. Japan,* **80,** 1309–1324.

——, K.-M. Kim, and S. Yang, 2000: Dynamical and boundary forcing characteristics of regional components of the Asian summer monsoon. *J. Climate,* **13,** 2461–2482.

——, J.-Y. Lee, K.-M. Kim, and I.-S. Kang, 2004: The North Pacific as a regulator of summertime climate over Eurasia and North America. *J. Climate,* **17,** 819–833.

Lau, N.-C., and E. O. Holopainen, 1984: Transient eddy forcing of the time-mean flow as identified by geopotential tendencies. *J. Atmos. Sci.,* **41,** 313–328.

——, and M. J. Nath, 1991: Variability of the baroclinic and barotropic transient eddy forcing associated with monthly changes in the midlatitude storm tracks. *J. Atmos. Sci.,* **48,** 2589–2613.

Lee, E., T. N. Chase, and B. Rajagopalan, 2008a: Highly improved predictive skill in the forecasting of the East Asian summer monsoon. *Water Resour. Res.,* **44,** W10422, doi:10.1029/2007WR06514.

——, ——, and ——, 2008b: Seasonal forecasting of East Asian summer monsoon based on oceanic heat sources. *Int. J. Climatol.,* **28,** 667–678.

Livezey, R. E., 1990: Variability of skill of long-range forecasts and implications for their use and value. *Bull. Amer. Meteor. Soc.,* **71,** 300–309.

——, 2003: Categorical events. *Forecast Verification: A Practitioner's Guide in Atmospheric Science,* I. T. Jolliffe and D. B. Stephenson, Eds., Wiley, 77–96.

Michaelsen, J., 1987: Cross-validation in statistical climate forecast model. *J. Climate Appl. Meteor.,* **26,** 1589–1600.

Nakamura, H., and A. Shimpo, 2004: Seasonal variations in the Southern Hemisphere storm tracks and jet streams as revealed in a reanalysis dataset. *J. Climate,* **17,** 1828–1844.

——, T. Sampe, Y. Tanimoto, and A. Shimpo, 2004: Observed associations among storm tracks, jet streams and midlatitude oceanic fronts. *Earth's Climate: The Ocean–Atmosphere Interaction, Geophys. Monogr.,* Vol. 147, Amer. Geophys. Union, 329–345.

——, ——, A. Goto, W. Ohfuchi, and S.-P. Xie, 2008: On the importance of midlatitude oceanic frontal zones for the mean state and dominant variability in the tropospheric circulation. *Geophys. Res. Lett.,* **35,** L15709, doi:10.1029/2008GL034010.

Nitta, T., 1987: Convective activities in the tropical western Pacific and their impact on the Northern Hemisphere summer circulation. *J. Meteor. Soc. Japan,* **65,** 373–390.

Qiu, B., 2003: Kuroshio extension variability and forcing of the Pacific decadal oscillations responses and potential feedback. *J. Phys. Oceanogr.,* **33,** 2465–2466.

——, and T. M. Joyce, 1992: Interannual variability in the mid- and low-latitude western North Pacific. *J. Phys. Oceanogr.,* **22,** 1062–1079.

——, and K. A. Kelly, 1993: Upper-ocean heat balance in the Kuroshio extension region. *J. Phys. Oceanogr.,* **23,** 2027–2041.

Reynolds, R. W., T. M. Smith, C. Liu, D. B. Chelton, K. S. Casey, and M. G. Schlax, 2007: Daily high-resolution-blended analyses for sea surface temperature. *J. Climate,* **20,** 5473–5496.

Rogerson, P. A., 2001: *Statistical Methods for Geography.* SAGE Publications, 136 pp.

Sampe, T., and S.-P. Xie, 2010: Large-scale dynamics of the meiyu-baiu rainband: Environmental forcing by the westerly jet. *J. Climate,* **23,** 113–134.

——, H. Nakamura, A. Goto, and W. Ohfuchi, 2010: Significance of a midlatitude SST frontal zone in the formation of a storm track and an eddy-driven westerly jet. *J. Climate,* **23,** 1793–1814.

Seo, K.-H., J.-H. Son, and J.-Y. Lee, 2011: A new look at changma: Atmosphere. *Korean Meteor. Soc.,* **21,** 109–121.

——, ——, S.-E. Lee, T. Tomita, and H.-S. Park, 2012: Mechanisms of an extraordinary East Asian summer monsoon event in July 2011. *Geophys. Res. Lett.,* **39,** L05704, doi:10.1029/2011GL050378.

——, J. Ok, J.-H. Son, and D.-H. Cha, 2013: Assessing future changes in the East Asian summer monsoon using CMIP5 coupled models. *J. Climate,* **26,** 7662–7675.

Shukla, J., 1998: Predictability in the midst of chaos: A scientific basis for climate forecasting. *Science,* **282,** 728–731, doi:10.1126/science.282.5389.728.

——, and D. A. Mooley, 1987: Empirical prediction of the summer monsoon rainfall over India. *Mon. Wea. Rev.,* **115,** 695–704.

Sperber, K. R., and T. Palmer, 1996: Interannual tropical rainfall variability in general circulation model simulations associated with the Atmospheric Model Intercomparison Project. *J. Climate,* **9,** 2727–2750.

Sun, J., H. Wang, and W. Yuan, 2008: Decadal variations of the relationship between the summer North Atlantic Oscillation and middle East Asian air temperature. *J. Geophys. Res.,* **113,** D15107, doi:10.1029/2007JD009626.

Sung, M.-K., W.-T. Kwon, H.-J. Baek, K.-O. Boo, G.-H. Lim, and J.-S. Kug, 2006: A possible impact of the North Atlantic Oscillation on the East Asian summer monsoon precipitation. *Geophys. Res. Lett.,* **33,** L21713, doi:10.1029/2006GL027253.

Vallis, G. K., and E. P. Gerber, 2008: Local and hemispheric dynamics of the North Atlantic Oscillation, annular patterns and the zonal index. *Dyn. Atmos. Oceans,* **44,** 184–212.

Wang, B., R. Wu, and X. Fu, 2000: Pacific–East Asian teleconnection: How does ENSO affect East Asian climate? *J. Climate,* **13,** 1517–1536.

——, ——, and K.-M. Lau, 2001: Interannual variability of the Asian summer monsoon: Contrasts between the Indian and the western North Pacific–East Asian monsoons. *J. Climate,* **14,** 4073–4090.

——, I.-S. Kang, and J.-Y. Lee, 2004: Ensemble simulations of Asian–Australian monsoon variability by 11 AGCMs. *J. Climate,* **17,** 803–818.

——, Q. Bao, B. Hoskins, G. Wu, and Y. Liu, 2008: Tibetan Plateau warming and precipitation changes in East Asia. *Geophys. Res. Lett.,* **35,** L14702, doi:10.1029/2008GL034330.

——, J. Liu, J. Yang, T. Zhou, and Z. Wu, 2009a: Distinct principal modes of early and late summer rainfall anomalies in East Asia. *J. Climate,* **22,** 3864–3875.

——, and Coauthors, 2009b: Advance and prospectus of seasonal prediction: Assessment of the APCC/CliPAS 14-model ensemble retrospective seasonal prediction (1980–2004). *Climate Dyn.,* **33,** 93–117.

——, B. Xiang, and J.-Y. Lee, 2013: Subtropical high predictability establishes a promising way for monsoon and tropical storm predictions. *Proc. Natl. Acad. Sci. USA,* **110,** 2718–2722, doi:10.1073/pnas.1214626110.

Webster, P. J., V. O. Magana, T. N. Palmer, J. Shukla, R. A. Tomas, M. Yanai, and T. Yasunari, 1998: Monsoons: Processes, predictability, and prospects for prediction. *J. Geophys. Res.,* **103** (C7), 14 452–14 510.

Wilks, D. S., 2006: *Statistical Methods in the Atmospheric Sciences.* 2nd ed. Academic Press, 630 pp.

WMO, 2010: Attachment II. *Global Aspects,* Vol. I, *Manual on the Global Data-Processing and Forecasting System,* World Meteorological Organization, WMO-485, II.8-1–II.8-17.

Wu, Z., B. Wang, J. Li, and F.-F. Jin, 2009: An empirical seasonal prediction model of the East Asian summer monsoon using ENSO and NAO. *J. Geophys. Res.,* **114,** D18120, doi:10.1029/2009JD011733.

Xie, S.-P., K. Hu, J. Hafner, H. Tokinaga, Y. Du, G. Huang, and T. Sampe, 2009: Indian Ocean capacitor effect on Indo–western Pacific climate during the summer following El Niño. *J. Climate,* **22,** 730–747.

Yamaura, Y., and Y. Tomita, 2011: Spatiotemporal differences in the interannual variability of baiu frontal activity in June. *Int. J. Climatol.,* **31,** 57–71.

Yang, S., K.-M. Lau, and K.-M. Kim, 2002: Variations of the East Asian jet stream and Asian–Pacific–American winter climate anomalies. *J. Climate,* **15,** 306–325.

Yim, S.-Y., J.-G. Jhun, R. Lu, and B. Wang, 2010: Two distinct patterns of spring Eurasian snow cover anomaly and their impacts on the East Asia summer monsoon. *J. Geophys. Res.,* **115,** D22113, doi:10.1029/2010JD01399.

Yun, K.-S., B. Ren, K.-J. Ha, J. C. L. Chan, and J.-G. Jhun, 2009: The 30–60-day oscillation in the East Asian summer monsoon and its time-dependent association with the ENSO. *Tellus,* **61A,** 565–578.